ChemComm

Accepted Manuscript

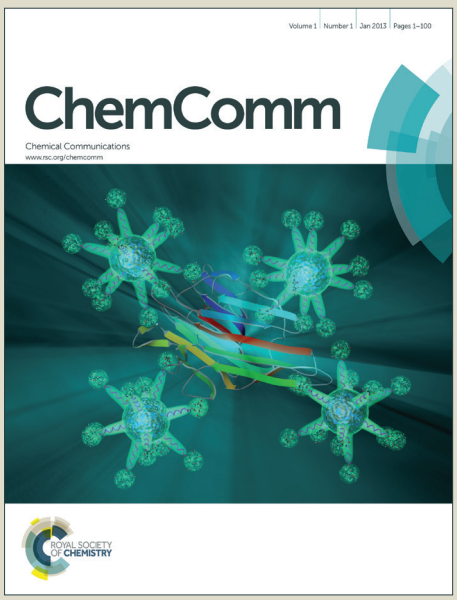

ROYAL SOCIETY OF CHEMISTRY

www.rsc.org/chemcomm

ChemComm

RSCPublishing

COMMUNICATION

Dopamine-Mo^{VI} complexation-assisted large-scale aqueous synthesis of single-layer MoS_2/carbon sandwich structure for ultrafast, long-life lithium-ion batteries

Cite this: DOI: 10.1039/x0xx00000x

Received 00th January 2012,
Accepted 00th January 2012

DOI: 10.1039/x0xx00000x

www.rsc.org/

Chenyang Zhao,[a] Junhua Kong,[a] Liping Yang,[b] Xiayin Yao,[a] Si Lei Phua[a] and Xuehong Lu*[a]

Single-layer MoS_2/carbon nanocomposites ($SLMoS_2$/C) are facilely prepared via a dopamine (DOPA)-Mo^{VI} complexation-assisted approach. The large interlayer spacing, sandwich structure and crumpled nanosheet morphology of $SLMoS_2$/C render it excellent electrochemical performances as a lithium-ion battery anode, showing a reversible capacity of 500 mAh/g at discharge rate of 5 A/g.

Lithium-ion batteries (LIBs) are promising power sources for high-power tools. However, to make the performance and cost of such tools viable for everyday consumer use, large-scale production of LIB electrodes with excellent rate capability and cycle life must be realized. MoS_2 has recently been identified as a promising LIB anode material.[1-3] Similar to graphite, the commercial anode material, in MoS_2 the atoms within a layer are covalently bonded while neighbor layers are held together by van der Waals forces. The weak interlayer interaction allows the intercalation of Li^+ into interlayer spaces.[4-6] Moreover, MoS_2 can be converted into Mo and Li_2S, providing substantial redox capacity.[7,8] Previous research has shown that MoS_2 nanoplates with large interlayer space exhibit excellent rate capability owing to the reduced barrier for Li^+ intercalation.[9,10] Single-layer and few-layer MoS_2 show further improved electrochemical performances because the enlarged surface area and shortened ion diffusion length.[11,12] Reversible capacity of MoS_2 could also be greatly improved by integrating MoS_2 with carbon materials due to enhanced electron transport and structural stability.[13-18] However, the synthesis of $SLMoS_2$/C is still a challenge.[19] Hydrothermal grwoth of MoS_2 with glucose typically gives a mixture of single-layer and few-layer MoS_2 in carbon.[20,21] Alhough electrospinning produces $SLMoS_2$/C with excellent properties, it has to use organic solvents.[22] Large-scale aqueous synthesis of $SLMoS_2$/C has not yet been realized.

DOPA has been widely used to prepare biomimetic adhesive coatings on various substrates via self-polymerization of DOPA in aqueous media.[23,24] A recent study revealed that polydopamine (PDOPA) coatings could be cacinated to layered carbon with electrical conductivities close to that of nitrogen-doped graphene.[25] Another interesting feature of DOPA is its complexation ability with various ligands, including molybdate (MoO_4^{2-}), a widely used precursor in MoS_2 synthesis. Enlightened by these findings, we developed a DOPA-Mo^{VI} complexation-assisted approach for large-scale aqueous synthesis of $SLMoS_2$/C. By simply mixing dopamine hydrochloride (DOPA-HCl) and sodium molybdate (Na_2MoO_4) aqueous solutions, DOPA-Mo^{VI} complex (DMC) are formed, which induces oligomerization of DOPA, yielding small DMC domains dispersed in DOPA oligomers. Subsequent hydrothermal growth of MoS_2 is thus confined, giving disordered $SLMoS_2$ embedded in polydopamine-derived carbon. The distance between adjacent $SLMoS_2$ layers is ~1.0 nm with a thin layer of carbon in between. Herein we report the structures and morphologies of the complex and resultant $SLMoS_2$/C as well as the formation mechanisms. Electrochemical properties of $SLMoS_2$/C-based LIB anode, including rate capability and cycling stability, are also demonstrated.

$SLMoS_2$/C was prepared by firstly mixing Na_2MoO_4 and DOPA-HCl aqueous solutions. Upon mixing the two colorless solutions, an orange-red suspension was formed (Fig. S1). The DOPA-HCl and Na_2MoO_4 solutions do not show any absorption in the wavelength region of 300 to 700 nm, whereas a broad absorption band is observed at 407.5 nm for the suspension (Fig. 1a), confirming the formation of DMC with Mo/DOPA ratio of 1:2,[26] i.e., the coordination number of Mo^{VI} is increased from four to six,[27] despite the feed molar ratio of Na_2MoO_4 to DOPA-HCl is ~1:3.5. FTIR spectra of DOPA-HCl, Na_2MoO_4 and DMC are shown in Fig. 1b (full spectra in Fig. S2). Na_2MoO_4 does not have characteristic absorption band in 1100-1650 cm^{-1} region, while for DOPA, absorption bands at 1342, 1320, 1189 and 1174 cm^{-1} are observed, which can be assigned to CH_2, C-O-H bending vibration and C-O, C-C stretching vibration, respectively. All these bands are absent in the DMC spectrum while new bands emerge at 1537 cm^{-1} and 1429 cm^{-1}, indicating the formation of indole structure.[28,29] X-ray photoelectron spectroscopy (XPS) studies show that the binding energiy of N 1s in DOPA is 402.1 eV (Fig. 1c), while the single peak splits into two peaks at 398.6 and 401.5 eV, respectively, for DMC (Fig. 1d), indicating the existence of secondary and tertiary amine groups.[30] The full XPS survey of DMC is provided in Fig. S3. The FTIR and XPS analyses indicate that oligomerization of DOPA occurs in the suspension, which involves cyclization of DOPA and assembly of DOPA units by covalent and non-covalent interactions.[31] Commonly PDOPA is spontaneously formed by pH-induced oxidative polymerization of DOPA at pH ≈ 8.3. In this case, the pH of the suspension is only 6. Thus, it is likely that while

DOPA donates its electrons to Mo^{VI} in DMC, the electron density on DOPA is reduced, inducing oxidative oligomerization of DOPA. It is also striking to see that DMC exhibits sea-island morphology with evenly distributed Mo-rich islands of ca. 4 nm (Fig. 1e and Fig. S4). The islands are surrounded by wrinkled layer structure, suggesting the sea is composed of DOPA oligomers,[25] as illustrated in Fig. 1f.

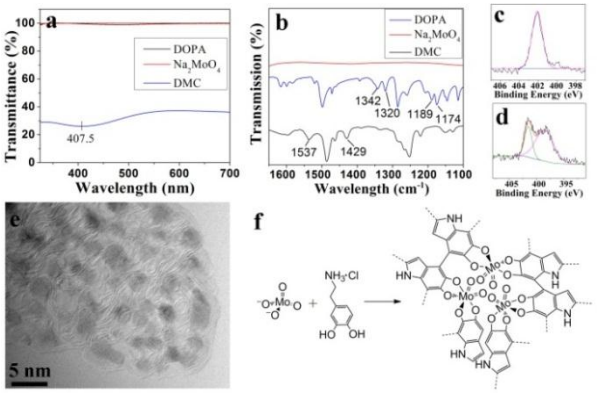

Fig. 1 (a) UV-Vis and (b) FTIR spectra of DOPA-HCl, Na_2MoO_4 and DMC; XPS N 1s spectra of (c) DOPA-HCl and (d) DMC; (e) TEM image and (f) structural illustration of DMC.

The suspension was then mixed with thioacetamide (TAA) and hydrothermally treated at 200 °C for 16 h. TAA acts as both reducing and vulcanizing agent to convert molybdate to MoS_2, while PDOPA were partially carbonized under hydrothermal conditions (Fig. S5). The hydrothermal product (DMC-HT) was annealed at 700 °C in Ar to yield $SLMoS_2/C$. The mass fractions of MoS_2 in DMC-HT and $SLMoS_2/C$ are 72 and 76 wt%, respectively (Fig. S6). Both DMC-HT (Fig. S7a) and $SLMoS_2/C$ (Fig. 2a) are porous agglomerates composed of crumpled nanoplates, similar to the morphology of reduced graphene oxide. Transmission electron microscopic (TEM) studies show that each nanoplate consists of 3-5 layers of disordered $SLMoS_2$ embedded in carbon (Fig. 2b and Fig. S7b). In DMC-HT, the distance between adjacent $SLMoS_2$ is around 1.05 nm, between which a fine line can be observed. It implies that some DOPA molecules intercalate into MoS_2 interlayer space, leading to a PDOPA-derived carbon layer sandwiched by $SLMoS_2$. The length of each $SLMoS_2$ is only 5 to 10 nm (Fig. 2c). After annealing, the sandwich structure can be observed more clearly. The length of $SLMoS_2$ is increased to 15-20 nm while the interlayer spacing is reduced to ~1.02 nm (Fig. 2d). X-ray diffraction (XRD) patterns of DMC-HT and $SLMoS_2/C$ are shown in Fig. 2e. For $SLMoS_2/C$, three distinct peaks at 2θ = 8.65°, 33.1° and 58.5° correspond to (002), (100) and (110) planes of MoS_2, respectively. These peaks are at slightly higher angle and much stronger than that of DMC-HT, indicating annealing-induced shrinkage in interlayer spacing and perfection of MoS_2 crystallites. The interlayer spacing of $SLMoS_2/C$ calculated from (002) peak (d =1.02 nm) is consistent with the TEM result, and much larger than that of bulk sample (JCPDS 37-1492, 2θ = 14.4°, d =0.62 nm). It is worth noting that there is a weak peak at 2θ =17.9° and its *d*-spacing (0.50 nm) is about half of that of MoS_2 interlayer spacing. This could be attributed to the spacing between adjacent $SLMoS_2$ and carbon layer, confirming the sandwich structure.[32] No peak corresponding to carbon is observed, implying the amorphous nature of the PDOPA-derived carbon. The Raman spectrum of $SLMoS_2/C$ is shown in Fig. 2f. Two characteristic peaks at 388 and 410 cm^{-1} are observed for the MoS_2 with a Δ value of 22 cm^{-1}, indicating that the nanosheets have either single-layer or few layer structure.[33]

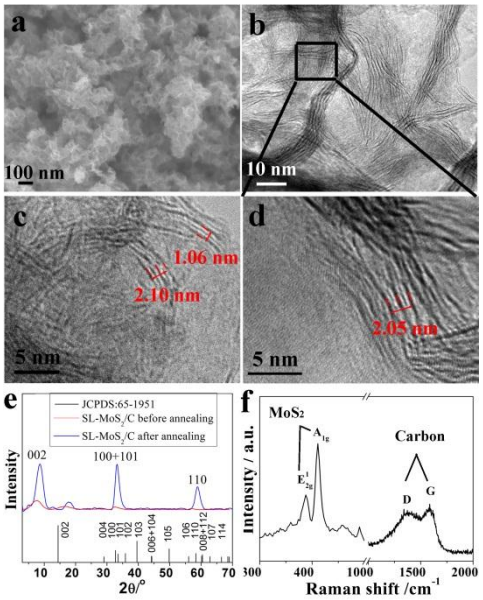

Fig. 2 (a) SEM, (b, d) TEM images and (f) Raman spectrum of $SLMoS_2/C$; (c) TEM image of DMC-HT; (e) XRD patterns of $SLMoS_2/C$ and DMC-HT.

Based on the data presented above, a structural evolution mechanism is proposed, as illustrated in Fig. 3. With the excessive amount of DOPA-HCl in the solution, MoO_4^{2-} form complex with DOPA, inducing oxidative oligmorization and leading to a precipitate in which DMC species are dispersed in PDOPA. In the subsequent hydrothermal process, PDOPA partially carbonize under high temperature and pressure, while the growth of MoS_2 is confined by surrounding PDOPA, facilitating the formation of disordered $SLMoS_2$ with limited size. Furthermore, some DOPA molecules in vicinity of Mo species intercalate into MoS_2 interlayer space, enabling the formation of $SLMoS_2/C$ sandwich structure. This facile process puts forward a generic strategy for large-scale production of metal oxide/sulfide ultrafine crystals embedded in carbon matrix. For verification, the complexation-assisted syntheses of Fe_3O_4/C and WO_2/C composites were conducted. As shown in Fig. S8-S9, the composites also exhibit sea-island morphologies with embedded Fe_3O_4 and WO_2 particles of ca. 7 nm and 4 nm, respectively.

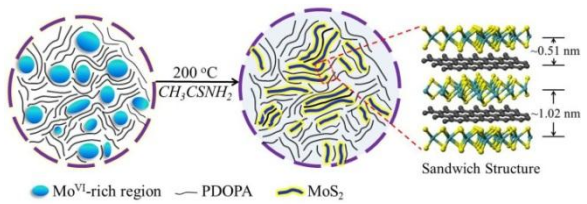

Fig. 3 Schematics showing structural and morphological evolutions of $SLMoS_2/C$.

Electrochemical properties of $SLMoS_2/C$ as a LIB anode are demonstrated in Fig. 4 and Fig. S10-S12. Fig. 4a shows its charge/discharge profiles at a curent density of 50 mA/g. In the first cycle, the $SLMoS_2/C$ anode delivers discharge capacity of 1678 mAh/g and charge capacity of 1072 mAh/g. The capacity loss between the 1st and the 2nd cycle could be attributed to the formation of SEI layer and the structure conversion during the first discharge.

The capacities are rapidly stabilized from the 2nd cycle onwards. The rate capability of the anode is shown in Fig. 4b. It delivers charge capacities of 1130, 1050, 955, 820, 675, 505 and 230 mAh/g at 0.05, 0.1, 0.2, 0.5 1.0, 2.0, 5.0 A/g, respectively, showing excellent rate capability. The charge capacity rebounds to 1210 mAh/g when the current is reset to 50 mA/g. The superior cycling stability of $SLMoS_2$/C at high current densities is demonstrated in Fig. 4c. At discharge rate of 5 A/g and charge rate of 1 A/g, the charge capacity gradually increases to 500 mAh/g at the 260th cycle, probably because cycling-induced activation of Li^+ pathway and expansion of defect sites that facilitates intercalation of more Li^+.[8,9,11,17] The capacity keeps at 400 mAh/g till the 800th cycle with Coulombic efficiency above 99%. The outstanding electrochemical performances are due to its unique structure and morphology. The small crystal size of $SLMoS_2$ shortens the Li^+ diffusion distance, and the large interlayer distance facilitates fast Li^+ intercalation and helps to relieve the strain caused by Li^+ intercalation. The sandwich structure enhances electron conduction and structural stability.[15] The crumpled nanosheet morphology provides large surface area, benefiting fast electron/ion transport.

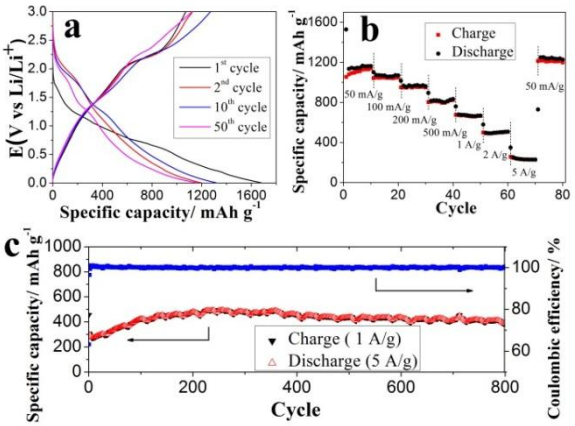

Fig. 4 (a) Charge/discharge profiles, (b) rate capability and (c) cycling performance at discharge rate of 5 A/g and charge rate of 1 A/g of the $SLMoS_2$/C anode.

Conclusions

With the assistance of DMC, large-scale aqueous synthesis of $SLMoS_2$/C is readily realized for the first time. Disordered $SLMoS_2$, with length of 20 nm, are randomly oriented in PDOPA-derived carbon matrix. The distance between adjacent $SLMoS_2$ is about 1.0 nm, with a carbon layer in between. These structural characteristics make $SLMoS_2$/C an excellent LIB anode material. A reversible capacity of 400 mAh/g can be achieved after cycling at a discharge rate of 5 A/g for 800 cycles. More importantly, this synthesis strategy is simple and scalable, and can be extended to prepare other metal oxide/sulfide ultrafine crystals embedded in carbon matrix.

Notes and references

[a] School of Materials Science and Engineering, Nanyang Technological University, 50 Nanyang Avenue, 639798, Singapore.

[b] Institute of Chemical and Engineering Sciences, A*STAR, 1 Pesek Road, Jurong Island, Singapore 627833, Singapore.

† Electronic Supplementary Information (ESI) available: [photo images, FTIR and XPS spectra of DOPA-HCl, Na_2MoO_4 and DMC; TEM images of DMC, DMC-HT, SL-MoS_2/C, Fe_3O_4/C and WO_2/C; XRD patterns of Fe_3O_4/C and WO_2/C; electrochemical properties of the $SLMoS_2$/C anode]. See DOI: 10.1039/c000000x/

references

1. M.-R. Gao, Y.-F. Xu, J. Jiang and S.-H. Yu, *Chem. Soc. Rev.*, 2013, **42**, 2986.
2. T. Stephenson, Z. Li, B. Olsen and D. Mitlin, *Energy Environ. Sci.*, 2014, **7**, 209.
3. X. Huang, Z. Zeng and H. Zhang, *Chem. Soc. Rev.*, 2013, **42**, 1934.
4. H. S. S. Ramakrishna Matte, A. Gomathi, A. K. Manna, D. J. Late, R. Datta, S. K. Pati and C. N. R. Rao, *Angew. Chem.*, 2010, **122**, 4153.
5. C. N. R. Rao and A. Nag, *Eur. J. Inorg. Chem.*, 2010, **2010**, 4244.
6. Z. Zeng, Z. Yin, X. Huang, H. Li, Q. He, G. Lu, F. Boey and H. Zhang, *Angew. Chem., Int. Ed.*, 2011, **50**, 11093.
7. X. Fang, X. Guo, Y. Mao, C. Hua, L. Shen, Y. Hu, Z. Wang, F. Wu and L. Chen, *Chem. - Asian J.*, 2012, **7**, 1013.
8. J. Xiao, X. Wang, X.-Q. Yang, S. Xun, G. Liu, P. K. Koech, J. Liu and J. P. Lemmon, *Adv. Funct. Mater.*, 2011, **21**, 2840.
9. H. Hwang, H. Kim and J. Cho, *Nano Lett.*, 2011, **11**, 4826.
10. H. Liu, D. Su, R. Zhou, B. Sun, G. Wang and S. Z. Qiao, *Adv. Energy Mater.*, 2012, **2**, 970.
11. K. Chang, D. Geng, X. Li, J. Yang, Y. Tang, M. Cai, R. Li and X. Sun, *Adv. Energy Mater.*, 2013, **3**, 839.
12. K. Chang and W. Chen, *J. Mater. Chem.*, 2011, **21**, 17175.
13. H. Yu, C. Zhu, K. Zhang, Y. Chen, C. Li, P. Gao, P. Yang and Q. Ouyang, *J. Mater. Chem. A*, 2014, **2**, 4551.
14. C. Lu, W.-w. Liu, H. Li and B. K. Tay, *Chem. Commun.* , 2014, **50**, 3338.
15. K. Chang and W. Chen, *Chem. Commun.* , 2011, **47**, 4252.
16. S. K. Das, R. Mallavajula, N. Jayaprakash and L. A. Archer, *J. Mater. Chem.*, 2012, **22**, 12988.
17. C. Zhao, J. Kong, X. Yao, X. Tang, Y. Dong, S. L. Phua and X. Lu, *ACS applied materials & interfaces*, 2014, **6**, 6392.
18. X. Cao, Y. Shi, W. Shi, X. Rui, Q. Yan, J. Kong and H. Zhang, *Small*, 2013, **9**, 3433.
19. G. Du, Z. Guo, S. Wang, R. Zeng, Z. Chen and H. Liu, *Chem. Commun.* , 2010, **46**, 1106.
20. K. Chang and W. Chen, *ACS Nano*, 2011, **5**, 4720.
21. K. Chang, W. Chen, L. Ma, H. Li, H. Li, F. Huang, Z. Xu, Q. Zhang and J.-Y. Lee, *J. Mater. Chem.*, 2011, **21**, 6251.
22. C. Zhu, X. Mu, P. A. van Aken, Y. Yu and J. Maier, *Angew. Chem., Int. Ed.*, 2014, **53**, 2152.
23. H. Lee, S. M. Dellatore, W. M. Miller and P. B. Messersmith, *Science*, 2007, **318**, 426.
24. L. Yang, S. L. Phua, J. K. H. Teo, C. L. Toh, S. K. Lau, J. Ma and X. Lu, *ACS Appl. Mater. Interfaces*, 2011, **3**, 3026.
25. J. Kong, W. A. Yee, L. Yang, Y. Wei, S. L. Phua, H. G. Ong, J. M. Ang, X. Li and X. Lu, *Chem. Commun.* , 2012, **48**, 10316.
26. K. Kustin and S.-T. Liu, *J. Am. Chem. Soc.*, 1973, **95**, 2487.
27. A. K. Duhme‐Klair, *Eur. J. Inorg. Chem.*, 2009, **2009**, 3689.
28. M. J. Sever, J. T. Weisser, J. Monahan, S. Srinivasan and J. J. Wilker, *Angew. Chem.*, 2004, **116**, 454.
29. L. Wang, D. Wang, Z. Dong, F. Zhang and J. Jin, *Small*, 2014, **10**, 998.
30. Z. Li, Z. Xu, X. Tan, H. Wang, C. M. B. Holt, T. Stephenson, B. C. Olsen and D. Mitlin, *Energy Environ. Sci.*, 2013, **6**, 871.
31. S. Hong, Y. S. Na, S. Choi, I. T. Song, W. Y. Kim and H. Lee, *Adv. Funct. Mater.*, 2012, **22**, 4711.
32. R. Bissessur and P. K. Liu, *Solid state ionics*, 2006, **177**, 191.
33. K.. Liu, W. Zhang, Y. Lee, Y. Lin, M. Chang, C. Su, C. Chang, H. Li, Y. Shi, H. Zhang, C. Lai and L. Li, *Nano letters*, 2012, **12**, 1538.